The Astrophysical Journal, 609:313–316, 2004 July 1

THE CHAOTIC BEHAVIOR OF THE BLACK HOLE SYSTEM GRS 1915+105

R. Misra,[1] K. P. Harikrishnan,[2] B. Mukhopadhyay,[3] G. Ambika,[4] and A. K. Kembhavi[1]

Received 2003 August 8; accepted 2004 March 15

ABSTRACT

A modified nonlinear time series analysis technique, which computes the correlation dimension D_2, is used to analyze the X-ray light curves of the black hole system GRS 1915+105 in all 12 temporal classes. For four of these temporal classes, D_2 saturates to $\approx$4–5, which indicates that the underlying dynamical mechanism is a low-dimensional chaotic system. Of the other eight classes, three show stochastic behavior, while five show deviation from randomness. The light curves for four classes that depict chaotic behavior have the smallest ratios of the expected Poisson noise to the variability ($<$0.05), while those for the three classes that depict stochastic behavior are the highest ($>$0.2). This suggests that the temporal behavior of the black hole system is governed by a low-dimensional chaotic system whose nature is detectable only when the Poisson fluctuations are much smaller than the variability.

Subject headings: accretion, accretion disks — black hole physics — X-rays: binaries — X-rays: individual (GRS 1915+105)

1. INTRODUCTION

Black hole X-ray binaries are variable on a wide range of timescales, from months to milliseconds. A detailed analysis of their temporal variability is crucial to the understanding of the geometry and structure of these high-energy sources. Such studies may eventually be used to test the relativistic nature of these sources and to understand the physics of the accretion process. The variability in different energy bands is generally quantified by computing the power spectrum, which is the amplitude squared of the Fourier transform. The power spectra give information about the characteristic frequencies of the system, which show up as either breaks or near-Gaussian peaks, i.e., quasi-periodic oscillation (QPO) in the spectra (e.g., Belloni et al. 2001; Tomsick & Kaaret 2001; Rodriguez et al. 2002). The shapes of the power spectra, combined with the observed frequency-dependent time lags between different energy bands, have put constraints on the radiative mechanisms and geometry of emitting regions (e.g., Nowak et al. 1999; Misra 2000; Cui 1999; Poutanen & Fabian 1999; Chakrabarti & Manickam 2000; Nobili et al. 2001).

These results are based on the response of the system to temporal variations whose origin is not clear. Important insight into the origin can be obtained by the detection and quantification of the possible nonlinear behavior of the fluctuations. For example, the presence of stochastic fluctuations would favor X-ray variations driven by variations of some external parameters (such as the mass accretion rate) or the possibility that active flares occur randomly. On the other hand, if the fluctuations can be described as a deterministic, chaotic system, then inner-disk instability or coherent flaring activity models will be the likely origin. A quantitative description of the temporal behavior can also be compared with time-dependent numerical simulations of the accretion process and will help examine the physical relevance of these simulations.

The non-Gaussian and nonzero skewness values of the temporal variation of the black hole system Cygnus X-1 suggested that the variations are nonlinear in nature (Thiel et al. 2001; Timmer et al. 2000; Maccarone & Coppi 2002). More rigorous tests were applied to the active galactic nucleus (AGN) Ark 564 (Gliozzi et al. 2002), which also suggested nonlinear behavior. Nonlinear time series (NLTS) analysis seems to be the most convenient tool for checking whether the origin of the variability is chaotic, stochastic, or a mixture of the two, and it has been adopted in several disciplines to study complex systems (e.g., the human brain, weather) and predict their immediate future (Schreiber 1999). This technique has also been used to analyze X-ray data of astrophysical sources. Based on an NLTS analysis of *EXOSAT* data, Voges et al. (1987) claimed that the X-ray pulsar Her X-1 was a low-dimensional chaotic system. However, Norris & Matilsky (1989) pointed out problems with that analysis, since the source has a strong periodicity and the data analyzed had a low signal-to-noise ratio. Lehto et al. (1993) used the NLTS technique to analyze *EXOSAT* light curves of several AGNs and found that only one, NGC 4051, showed signs of low-dimensional chaos. A similar analysis on the noise-filtered *Tenma* satellite data of Cyg X-1 suggested that the source may be a low-dimensional chaotic system with large intrinsic noise (Unno et al. 1990). These analyses were hampered by a small number of data points ($\lesssim$1000) in the light curve and/or noise. Hence, the reported detection of low-dimensional chaos was only possible by rather subjective comparison of the results of the data analysis with those from simulated data of chaotic systems with noise.

The Galactic microquasar GRS 1915+105 is a highly variable black hole system. It shows a wide range of variability (Chen et al. 1997; Paul et al. 1997; Belloni et al. 1997), which required Belloni et al. (2000) to classify its behavior into no fewer than 12 temporal classes. In this work, our motivation is to determine the temporal property of this source by using a modified NLTS analysis for each of these 12 classes. The different kinds of variability and its brightness (the average *RXTE* PCA count rate ranges from 5000 to 32,000 counts s^{-1}) make this source ideal ones for the detection of chaotic behavior.

[1] Inter-University Centre for Astronomy and Astrophysics, Post Bag 4, Ganeshkhind, Pune 411 007, India; rmisra@iucaa.ernet.in.
[2] Department of Physics, Cochin College, Cochin 682 002, India.
[3] Astronomy Division, P.O. Box 3000, University of Oulu, FIN-90014 Oulu, Finland.
[4] Department of Physics, Maharajas College, Cochin 682 011, India.

In the next section we describe the technique used to determine the correlation dimension. The results of the analysis are presented in § 3, while in § 4 the work is summarized and discussed.

2. THE NONLINEAR TIME-SERIES ANALYSIS

The algorithm normally employed in this analysis (Grassberger & Procaccia 1983) aims at creating an artificial (or pseudo-) space of dimension M with delay vectors constructed by splitting a scalar time series $s(t)$ with delay time τ as

$$\boldsymbol{x}(t) = [s(t), s(t+\tau), \ \ldots, \ s(t+(M-1)\tau)]. \quad (1)$$

The correlation function is the average number of data points within a distance R from a data point,

$$C_M(R) \equiv \lim_{N\to\infty} \frac{1}{N(N-1)} \sum_{i}^{N} \sum_{j,j\neq i}^{N} H\left(R - \left|\boldsymbol{x}_i - \boldsymbol{x}_j\right|\right), \quad (2)$$

where $\boldsymbol{x}_j$ is the position vector of a point belonging to the attractor in the M-dimensional space, N is the number of reconstructed vectors, and H is the Heaviside step function. The fractional dimension $D_2(M)$ is defined as

$$D_2 \equiv \lim_{R\to 0} \frac{d \log C_M(R)}{d \log (R)} \quad (3)$$

and is essentially the scaling index of $C_M(R)$ variation with R. The fractal dimension $D_2(M)$ can be used to differentiate between different temporal behavior, since for an uncorrelated stochastic system, $D_2 \approx M$, while for a chaotic system, $D_2(M) \approx$ constant for M greater than a certain dimension $M_{\max}$.

For a finite-duration light curve, there are two complications that hinder the successful computation of $D_2(M)$. First, for small values of R, $C_M(R)$ is of order unity, and the result there would be dominated by Poisson noise. Second, for large values of R, $C_M(R)$ will saturate to the total number of data points. Usually, these two effects are avoided in the $\log C_M(R)$ versus $\log R$ plot, and the slope D_2 is obtained from the linear part of the curve. However, such an exercise is subjective, especially for high dimensions. Here, we use a numerical scheme to compute D_2, which takes into account the above effects and at the same time optimizes the maximum use of the available data. The details of the method and several tests of its validity will be presented elsewhere (R. Misra et al. 2004, in preparation). Briefly, the technique involves converting the original light curve to a uniform deviate and redefining the correlation function $C_M(R)$ as the average number of data points within an M cube (instead of an M sphere) of length R around a data point. Only those M cubes are considered that are within the embedding space, ensuring that there are no edge effects due to limited data points. This imposes a maximum value of $R < R_{\max}$ for which $C_M(R)$ can be computed. To avoid the Poisson noise–dominated region, only results from R greater than an $R_{\min}$ are taken into consideration, such that the average $C(R_{\min}) > 1$, where the Poisson noise would approximately be $1/(N_c)^{1/2}$. Typically $C_M(R)$ is computed for 10 different values of R between $R_{\min}$ and $R_{\max}$, the logarithmic slope for each point is computed, and the average is taken to be $D_2(M)$. The error on $D_2(M)$ is estimated to be the mean standard deviation around this average. It should be noted that there often exists a critical $M_{\rm cr}$ for which $R_{\max} \approx R_{\min}$, and no significant result can then be obtained for $M > M_{\rm cr}$. Figure 1*a* shows the $D_2(M)$ curve for a time series generated from random numbers and for the well-known analytical low-dimensional chaotic system, the Lorenz system. The total number of data points used to generate both curves is 30,000, and the number of random centers used is $N_c = 2000$. As expected, the D_2 plot for the random data is consistent with the $D_2 = M$ curve, while the plot for the Lorenz system shows significant deviation and saturates at $M \approx 3$ to a $D_2 \approx 2$, which is close to the known value of 2.04. The random data and the low-dimensional chaotic system can clearly be distinguished in this scheme.

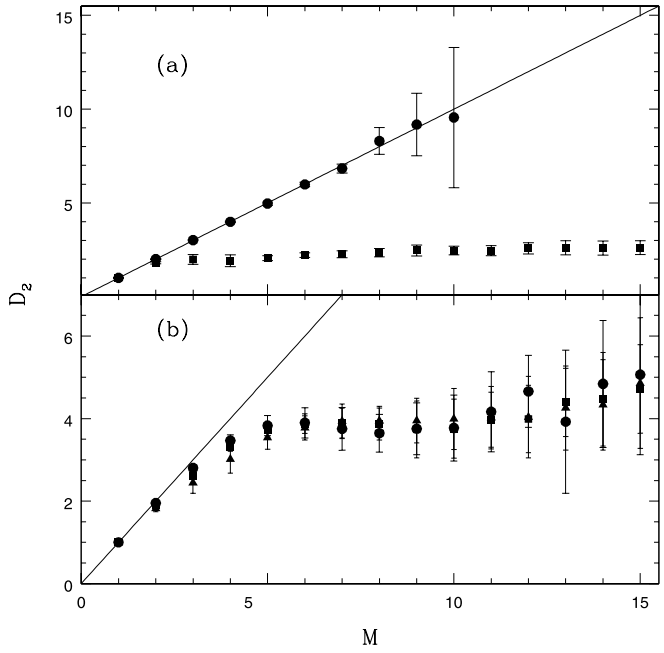

FIG. 1.—(*a*) D_2 vs. M for random points (*circles*) and for a Lorenz system (*squares*). For both curves the number of points used is 30,000, and the number of centers used in the computation is 2000. The straight line represents the $D_2 = M$ case, which is the expected result for random variation. (*b*) D_2 vs. M for GRS 1915+105 data obtained during class κ for three different values of the delay time: $\tau = 15$ s (*triangles*), 25 s (*squares*), and 100 s (*circles*).

3. RESULTS

The temporal properties of GRS 1915+105 have been classified into 12 different classes by Belloni et al. (2000), who also present the observational dates and identification number of the *RXTE* data they had used to make the classification. Here, we have chosen a representative data set for each class and extracted a few continuous data streams (≈3000 s long) from it. The observation IDs (ObsIDs) of the data used in this work are tabulated in Table 1. The light curves were generated with a resolution of 0.1 s, resulting in ≈30,000 data points for each of them and ≈1500 counts per bin. Light curves with finer time resolution are Poisson noise–dominated, while larger binning gives too few data points.

In general, $D_2(M)$ is proportional to τ when τ is small and saturates (i.e., it is nearly invariant) for τ greater than a critical value, and it is this saturated value that is the correct estimate of $D_2(M)$. As an example, the $D_2(M)$ curves for different values of τ are plotted in Figure 1*b*, where it can be seen that the curve is similar within error bars for $\tau = 15$, 25, and 100 s. For all the data analyzed here, the critical $\tau <$ 5–20 s, and hence the saturated curve (typically for $\tau \approx 50$ s) is considered.

TABLE 1
OBSERVATION TABLE

ObsID (1)	Class (2)	$\langle S \rangle$ (3)	rms (4)	$\langle \mathrm{PN} \rangle$ (5)	$\langle \mathrm{PN} \rangle$/rms (6)	Behavior (7)
10408-01-10-00.....	β	1917	1016	43.8	0.04	C
20402-01-37-01.....	λ	1493	1015	38.6	0.04	C
20402-01-33-00.....	κ	1311	800	36.2	0.04	C
10408-01-08-00.....	μ	3026	999	55	0.06	C
20402-01-45-02.....	θ	1740	678	41.7	0.06	NS
10408-01-40-00.....	ν	1360	462	36.9	0.08	NS
20402-01-03-00.....	ρ	1258	440	35.5	0.08	NS
20187-02-01-00.....	α	582	244	24.1	0.10	NS
10408-01-17-00.....	δ	1397	377	37.4	0.10	NS
20402-01-56-00.....	γ	1848	185	43.0	0.23	S
10408-01-22-00.....	χ	981	118	31.3	0.27	S
10408-01-12-00.....	ϕ	1073	118	32.7	0.28	S

NOTES.—Col. (1): *RXTE* ObsID from which the data has been extracted. Col. (2): Temporal class of the system in the classification given by Belloni et al. (2000). Col. (3): The average counts in the light curve $\langle S \rangle$. Col. (4): The rms variation in the light curve rms . Col. (5): The expected Poisson noise variation, $\langle \mathrm{PN} \rangle \equiv \langle S \rangle^{1/2}$. Col. (6): The ratio of the expected Poisson noise to the actual rms variation. Col. (7): The behavior of the system, as derived from the D_2 vs. M curves (C: chaotic behavior; NS: Nonstochastic behavior [i.e., the D_2 vs. M curve deviates slightly from random or stochastic behavior]; S: stochastic or random behavior).

It has been verified that the $D_2(M)$ curves for two separate light curves for the same class are similar to within the error bars. This shows that, as expected, the temporal behavior of the system is more or less stationary for the same class. Hence, such curves can be averaged to obtain a statistically more significant result.

Figure 2 shows the $D_2(M)$ curves for seven temporal classes. For four classes (λ, κ, β, and μ) the curves show clear deviation from random behavior. For λ and κ there is saturation of $D_2 \approx 5$ for $M > 8$. For β and μ, the increase in D_2 is less than 1 when M increases from 8 to 15. Thus, these classes can be classified unambiguously as chaotic systems with correlation dimension less than 5, while the behavior of the class ϕ is identical to a stochastic light curve. Classes α and ρ show some deviation from stochastic behavior, and hence this behavior, which is also seen in classes θ, ν, and δ, is named "nonstochastic" in this work. As discussed below, these classes may be inferred to be low-dimensional chaotic systems based on comparison with results from simulated data of chaotic systems with additional noise. Similar comparisons were made to infer the chaotic behavior of Cyg X-1 (Unno et al. 1990) and NGC 4051 (Lehto et al. 1993). We show in the last column of Table 1 the classification of all 12 classes into one

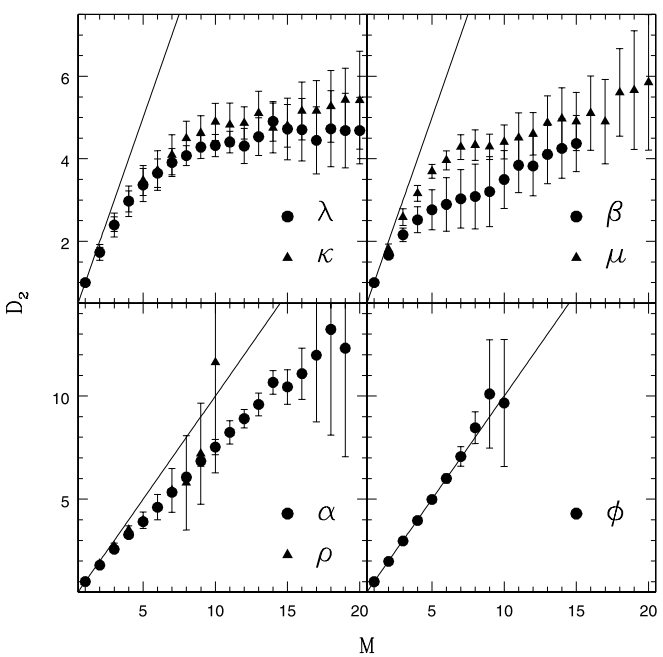

FIG. 2.— D_2 vs. M for GRS 1915+105 data obtained during seven temporal classes. Classes κ, μ, β, and λ exhibit chaotic behavior. Class ϕ is stochastic, while α and ρ show some departure from stochastic behavior.

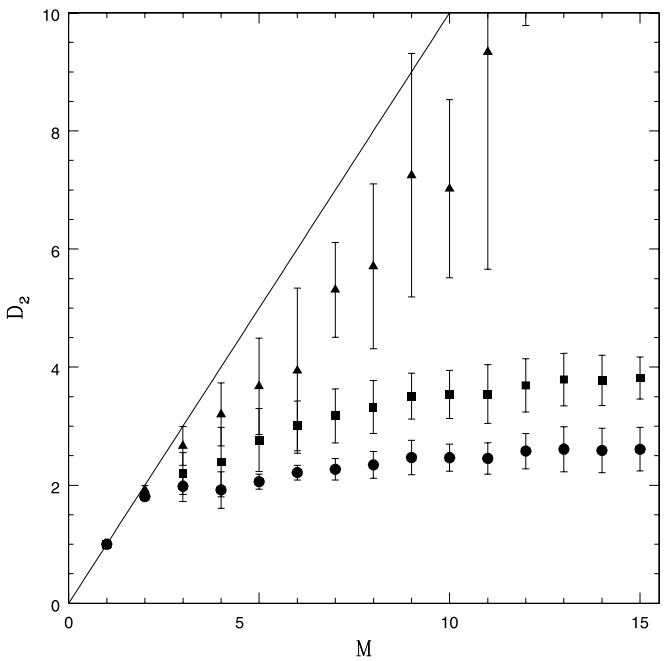

FIG. 3.—Effect of Poisson noise on the analysis using simulated rescaled Lorenz system data with Poisson noise. The D_2 vs. M curve for a Lorenz system is shown by circles, while the squares (triangles) are curves for rescaled Lorenz system data corresponding to the expected Poisson noise in the β (γ) class of GRS 1915+105.

of three categories: chaotic, nonstochastic, or stochastic. We list in Table 1 the average counts $\langle S \rangle$, the rms variation, the expected Poisson noise $\langle \mathrm{PN} \rangle \equiv \langle S \rangle^{1/2}$, and the ratio of the expected Poisson noise to the actual rms value. It can be seen that there is a strong correlation between the inferred behavior of the system and the ratio of the expected Poisson noise to the rms values. This indicates that Poisson noise is affecting the analysis. To estimate the effect of Poisson noise, we consider the Lorenz system points $S_{\mathrm{L}}(t)$ and rescale it by $S_{\mathrm{LR}} = AS_{\mathrm{L}}(t) + B$. A light curve is then simulated using S_{LR} from the corresponding Poisson noise distributions. The constants A and B were chosen such that the simulated light curve had the same average count and rms variation as the two extreme cases for the GRS 1915+105 data for the β and γ classes. The results of the NLTS analysis are shown in Figure 3, where it can be seen that even for the β-like case in which the ratio of the expected Poisson noise to rms variation is only 4%, the D_2 versus M curve saturates at a higher value than that of the original no-noise data points. This implies that the correlation dimension of $\approx$4 inferred from the analysis of the classes showing chaotic behavior (Fig. 2) is an overestimation due to the inherent Poisson noise in the data. For larger Poisson noise fractions, the curve no longer saturates, and it becomes qualitatively similar to that obtained for the nonstochastic case.

4. DISCUSSION

The saturation of the correlation dimension $D_2 \approx 4$–5 for four of the temporal classes clearly indicates that the underlying dynamic mechanism that governs the variability of the black hole system is a low-dimensional, chaotic one. As indicated by simulations of the Lorenz system with noise, the effect of Poisson noise in the data is to increase the D_2 values. Hence, the real dimension of the system is probably smaller than the $D_2 \approx 4$–5 that is obtained here. In fact, it is possible that the temporal behavior of the black hole system is always governed by a low-dimensional, chaotic system but is undetectable when Poisson noise affects the analysis.

Alternatively, there may be a stochastic component to the variability that dominates for certain temporal classes. The two scenarios may be distinguished, and better quantitative estimates of the correlation dimension may be obtained, by appropriate noise filtering of the data and/or appropriate averaging of the different light curves. Much longer ($\approx$30,000 s long) continuous data streams sampled at 1 s resolution would decrease Poisson noise and hence provide a better quantitative measure of D_2. However, such long data streams are currently not available, and merging noncontinuous light curves will require sophisticated gap-filling techniques that might give rise to spurious results.

The variability of GRS 1915+105 can be interpreted as being the manifestation of transitions between three spectral states (Belloni et al. 2000), one of which (the so-called soft state) is a long-term canonical state observed in other black hole systems like Cygnus X-1, which do not show such high-amplitude variability. It is attractive to identify these spectral states as fixed points, which for GRS 1915+105 become unstable, giving rise to the observed chaotic behavior, which may also account for the ringlike movement of the system in color-color space (Vilhu & Nevalainen 1998). The above hypothesis may be verified by future characterization of the chaos in GRS 1915+105. Note that GRS 1915+105 spends most of its time in the χ-class, whose variability is similar to that observed in other black hole systems like Cygnus X-1. However, as shown in this work, Poisson noise affects the analysis for the χ-class, and the $D_2(M)$ values reflect stochastic behavior. This may be the reason why earlier different nonlinear analysis of Cygnus X-1 data, while showing nonlinearity (Timmer et al. 2000; Thiel et al. 2001), did not conclusively reveal chaotic behavior.

The identification of the temporal behavior of the black hole system as chaotic has opened a new window toward the understanding of the origin and nature of their variability. The present analysis can be extended to characterize the chaotic behavior. Using the minimum required phase-space dimension, the data can be projected into different two-dimensional planes, which will reveal the structure of the attractor and help to identify any possible centers of instability in the system. Further, dynamical invariants, for example, the full Lyapunov spectrum and multifractal dimensions, can also be computed. Recently, Winters et al. (2003) have studied and quantified the chaotic flow in magnetohydrodynamic simulations of the mass accretion processes that are believed to be happening in black hole systems. The measured chaos parameters, such as the largest Lyapunov exponent, for such simulations can be compared with those obtained from the light curve of black hole systems to validate such simulations and enhance our understanding of these systems. Note that such analysis can practically be applied only after the identification of the minimum phase-space dimension, which in turn usually requires the computation of $D_2(M)$.

G. A. and K. P. H. acknowledge the hospitality and the facilities in IUCAA. B. M. thanks the Academy of Finland grant 80750 for support.

REFERENCES

Belloni, T., Klein-Wolt, M., Méndez, M., van der Klis, M., & van Paradijs, J. 2000, A&A, 355, 271
Belloni, T., Méndez, M., King, A. R., van der Klis, M., & van Paradijs, J. 1997, ApJ, 479, L145
Belloni, T., Méndez, M., & Sánchez-Fernández, C. 2001, A&A, 372, 551
Chakrabarti, S. K., & Manickam, S. G. 2000, ApJ, 531, L41
Chen, X., Swank, J. H., & Taam, R. E. 1997, ApJ, 477, L41
Cui, W. 1999, ApJ, 524, L59
Gliozzi, M., Brinkmann, W., Räth, C., Papadakis, I. E., Negoro, H., & Scheingraber, H. 2002, A&A, 391, 875
Grassberger, P., & Procaccia, I. 1983, Physica D, 9, 189
Lehto, H. J., Czerny, B., & McHardy, I. M. 1993, MNRAS, 261, 125
Maccarone, T. J., & Coppi, P. S. 2002, MNRAS, 336, 817
Misra, R. 2000, ApJ, 529, L95
Nobili, L., Belloni, T., Turolla, R., & Zampieri, L. 2001, Ap&SS Suppl., 276, 217
Norris, J. P., & Matilsky, T. A. 1989, ApJ, 346, 912
Nowak, M. A., Vaughan, B. A., Wilms, J., Dove, J. B. & Begelman, M. C. 1999, ApJ, 510, 874
Paul, B., et al. 1997, A&A, 320, L37
Poutanen, J., & Fabian, A. C. 1999, MNRAS, 306, L31
Rodriguez, J., Durouchoux, P., Mirabel, I. F., Ueda, Y., Tagger, M., & Yamaoka, K. 2002, A&A, 386, 271
Schreiber, T. 1999, Phys. Rep., 308, 1
Thiel, M., Romano, M., Schwarz, U., Kurths, J., Hasinger, G., & Belloni, T. 2001, Ap&SS Suppl., 276, 187
Timmer, J., et al. 2000, Phys. Rev. E, 61, 1342
Tomsick, J. A., & Kaaret, P. 2001, ApJ, 548, 401
Unno, W., et al. 1990, PASJ, 42, 269
Vilhu, O., & Nevalainen, J. 1998, ApJ, 508, L85
Voges, W., Atmanspacher, H., & Scheingraber, H. 1987, ApJ, 320, 794
Winters, W. F., Balbus, S. A., & Hawley, J. F. 2003, MNRAS, 340, 519